Supplemental Material

Coherence entropy during propagation through complex media

Xingyuan Lu[1,5], Zhuoyi Wang[1,5], Qiwen Zhan[2,✉], Yangjian Cai[3,4,✉], Chengliang Zhao[1,✉]

[1]*School of Physical Science and Technology, Jiangsu Key Laboratory of Frontier Material Physics and Devices, Soochow University, Suzhou 215006, China.*
[2]*School of Optical-Electrical and Computer Engineering, University of Shanghai for Science and Technology, Shanghai 200093, China.*
[3]*Shandong Provincial Engineering and Technical Center of Light Manipulations & Shandong Provincial Key Laboratory of Optics and Photonic Device, School of Physics and Electronics, Shandong Normal University, Jinan 250358, China.*
[4]*Joint Research Center of Light Manipulation Science and Photonic Integrated Chip, East China Normal University, Shanghai 200241, China.*
[5]*These authors contributed equally: Xingyuan Lu, Zhuoyi Wang.*

Supplemental Equations

When a quasi-monochromatic light passes through a no-energy-loss optical channel, both the spatial distribution and polarization can be perturbed, and the light field may be deformed or may even evolve into partially coherent and partially polarized light field. Modal decomposition is a powerful tool for investigating the evaluation of such a light field. The fundamental theory has been well introduced in the literature[1,2,49,50]. The invariant was quantitatively investigated in a general one-sided spatial transmission channel[19]. The investigation revealed the invariance of the vector quality factor (or polarization degree) in a unitary channel for a coherent vector beam via the adjustment of the basis of coherent modal decomposition. However, the polarization and spatial degrees of freedom (DoF) may be coupled during propagation[1]. Further experimental evidence, such as the entropy conversion experiment[28-30], indicate that the beam coherence-polarization (BCP) matrix combines the properties of a vector partially coherent light field, as mentioned in a previous report[32]. Thus, by applying the modal decomposition on the BCP matrix, we performed an analysis using a partially coherent and partially polarized light beam with diagonal BCP matrix. The overall coherence entropy of the light field and its robustness were investigated. It was found that, for the scalar case and in a unitary channel, the mode-weights and corresponding coherence entropy can be reconstructed. For the vector case, the modal decomposition of diagonal coherence-polarization matrix can be simplified as that of a scalar cross-spectral density defined with $W_{eq} = W_{xx} + W_{yy}$ [33]. Assuming that two polarizations share the same set of orthogonal spatial basis, the overall mode-weights for a light source with a diagonal BCP matrix remain consistent during propagation in a unitary channel. The premise for both scalar and vector cases is projecting the cross-spectral density and BCP matrix onto an appropriate orthogonal vector and spatial basis.

I. Scalar partially coherent beam

According to Mercer's theorem[35], for a continuous, Hermitian, non-negative definite

Hilbert–Schmidt kernel that is not identically zero, the cross-spectral density may be reformed with modal decomposition, as shown below:

$$W_0(\mathbf{r}_1, \mathbf{r}_2) = \sum_n \lambda_n \phi_n^*(\mathbf{r}_1)\phi_n(\mathbf{r}_2). \tag{S1}$$

Here, the series is absolutely and uniformly convergent. The frequency is omitted for brevity under the premise of quasi-monochromatic light. Thus, the partially coherent beam just means spatially partially coherent. Further, ϕ_n is an eigenfunction, and the corresponding coefficient is λ_n, which can be calculated using the homogeneous Fredholm integral equation:

$$\int W_0(\mathbf{r}_1, \mathbf{r}_2)\phi_n(\mathbf{r}_1)d\mathbf{r}_1 = \lambda_n \phi_n(\mathbf{r}_2). \tag{S2}$$

The hermiticity, i. e. $W_0(\mathbf{r}_2, \mathbf{r}_1) = \mathrm{W}_0^*(\mathbf{r}_1, \mathbf{r}_2)$, and non-negative definiteness of $W_0(\mathbf{r}_1, \mathbf{r}_2)$ ensures $\lambda_n \geq 0$. The orthogonal nature ensures that $\langle \phi_n | \phi_m \rangle_{m \neq n} = 0$.

$$\int \phi_n^*(\mathbf{r})\phi_m(\mathbf{r})\mathbf{dr} = \delta_{mn}, \tag{S3}$$

where δ_{mn} is the Kronecker symbol and $\delta_{mn} = 0$ only when $m \neq n$.

We consider a general partially coherent light field of an ensemble of function $\{U(\mathbf{r})\}$, each member of which is a superposition of eigenfunctions, written as $U(\mathbf{r}) = \sum_n \alpha_n \phi_n(\mathbf{r})$. Here, α_n is a random coefficient of the corresponding eigenfunctions $\phi(\mathbf{r})$. The cross-spectral density is then written as[2]:

$$W_0(\mathbf{r}_1, \mathbf{r}_2) = \langle U^*(\mathbf{r}_1)U(\mathbf{r}_2) \rangle = \sum_n \sum_m \langle \alpha_n^* \alpha_m \rangle \phi_n^*(\mathbf{r}_1)\phi_m(\mathbf{r}_2), \tag{S4}$$

where $\langle\ \rangle$ means ensemble average. Given that the coefficient is statistically independent, that is

$$\langle \alpha_n^* \alpha_m \rangle = \lambda_{mn}\delta_{mn}, \tag{S5}$$

then,

$$W_0(\mathbf{r}_1, \mathbf{r}_2) = \sum_n \lambda_n \phi_n^*(\mathbf{r}_1)\phi_n(\mathbf{r}_2). \tag{S6}$$

This is consistent with Eq. (S1) and $\lambda_n = \langle \alpha_n^* \alpha_n \rangle$.

In scalar cases, we do not consider the polarization modulation. After the partially coherent light passes through a unitary channel with transmission matrix T, the cross-spectral density is

$$W_T(\boldsymbol{\rho}_1, \boldsymbol{\rho}_2) = \sum_n \lambda_n' \phi_n'^*(\boldsymbol{\rho}_1)\phi_n'(\boldsymbol{\rho}_2). \tag{S7}$$

Because of the unitary nature of T, that is $T^\dagger = T^{-1}$, the basis $|\phi_n'\rangle = T|\phi_n\rangle$ is still orthogonal as

$$\langle \phi_n' | \phi_m' \rangle_{m \neq n} = \langle \phi_n | T^\dagger T | \phi_m \rangle_{m \neq n} = \langle \phi_n | \phi_m \rangle_{m \neq n} = 0. \tag{S8}$$

The modal decomposition can then be written as

$$\int W_T(\boldsymbol{\rho}_1, \boldsymbol{\rho}_2)\phi_n'(\boldsymbol{\rho}_1)d\boldsymbol{\rho}_1 = \lambda_n \phi_n'(\boldsymbol{\rho}_2). \tag{S9}$$

Here, mode-weights $\{\lambda_n\}$ are consistent, and thus, the coherence entropy defined with $S = -\sum_n \lambda_n \log_N (\lambda_n)$ remains consistent during propagation under the premise of unitary optical channel. Note that the mode-weights $\{\lambda_n\}$ are globally normalized. Some representative

examples are given below.

1. Orthogonal dual-mode light field.

For brevity, we first consider a light field containing two incoherent orthogonal spatial modes $U_1(\mathbf{r})$ and $U_2(\mathbf{r})$, written as $U_1(\mathbf{r}) = \alpha_1\phi_1(\mathbf{r})$ and $U_2(\mathbf{r}) = \alpha_2\phi_2(\mathbf{r})$. Then, the cross-spectral density will be

$$W_0(\mathbf{r}_1, \mathbf{r}_2) = \langle U^*(\mathbf{r}_1)U(\mathbf{r}_2)\rangle = U_1^*(\mathbf{r}_1)U_1(\mathbf{r}_2) + U_2^*(\mathbf{r}_1)U_2(\mathbf{r}_2)$$
$$= \lambda_1\phi_1^*(\mathbf{r}_1)\phi_1(\mathbf{r}_2) + \lambda_2\phi_2^*(\mathbf{r}_1)\phi_2(\mathbf{r}_2), \quad \text{(S10)}$$

where $\lambda_1 = \langle\alpha_1^*\alpha_1\rangle$ and $\lambda_2 = \langle\alpha_2^*\alpha_2\rangle$. When the light source propagates through a unitary optical system, two modes evolve into

$$|U_1'\rangle = T|U_1\rangle = \alpha_1 T|\phi_1\rangle = \alpha_1|\phi_1'\rangle,$$
$$|U_2'\rangle = T|U_2\rangle = \alpha_2 T|\phi_2\rangle = \alpha_2|\phi_2'\rangle, \quad \text{(S11)}$$

where $|U_i'\rangle$ denotes the modes on the propagation plane and $|\phi_i'\rangle$ is corresponding orthogonal basis ($i = 1,2$). The unitary matrix T ensures the orthogonal nature of the new basis, that is $\langle\phi_1'|\phi_2'\rangle = \langle\phi_1|T^\dagger T|\phi_2\rangle = \langle\phi_1|\phi_2\rangle = 0$. Then,

$$W_T(\boldsymbol{\rho}_1, \boldsymbol{\rho}_2) = \langle U'^*(\boldsymbol{\rho}_1)U'(\boldsymbol{\rho}_2)\rangle = \lambda_1\phi_1'^*(\boldsymbol{\rho}_1)\phi_1'(\boldsymbol{\rho}_2) + \lambda_2\phi_2'^*(\boldsymbol{\rho}_1)\phi_2'(\boldsymbol{\rho}_2), \quad \text{(S12)}$$

where the mode-weights $\{\lambda_n\}$ (n = 1 and 2) remain constant. If we choose a wrong basis $|\phi_{wn}'\rangle$, we will require a higher number of modes to characterize $W_T(\boldsymbol{\rho}_1, \boldsymbol{\rho}_2)$:

$$W_T(\boldsymbol{\rho}_1, \boldsymbol{\rho}_2) = \lambda_{w1}\phi_{w1}'^*(\boldsymbol{\rho}_1)\phi_{w1}'(\boldsymbol{\rho}_2) + \lambda_{w2}\phi_{w2}'^*(\boldsymbol{\rho}_1)\phi_{w2}'(\boldsymbol{\rho}_2)$$
$$+\lambda_{w3}\phi_{w3}'^*(\boldsymbol{\rho}_1)\phi_{w3}'(\boldsymbol{\rho}_2) + \lambda_{w4}\phi_{w4}'^*(\boldsymbol{\rho}_1)\phi_{w4}'(\boldsymbol{\rho}_2) ..., \quad \text{(S13)}$$

where the mode-weights $\{\lambda_{wn}\}$ are global normalized. Thus, the coherence entropy defined as $S = -\sum_n \lambda_{wn}\log_N(\lambda_{wn})$ changes. This is consistent with the conclusion of a previous report[19].

2. Multi-mode partially coherent light.

In the main manuscript, we consider a general case, that is the partially coherent light constructed with multi modes (in total M) and $U_i(\mathbf{r}) = \sum_n \alpha_{in}\phi_n(\mathbf{r})$ where $\{\alpha_{in}\}$ are statistically independent.

$$W_0(\mathbf{r}_1, \mathbf{r}_2) = \langle U^*(\mathbf{r}_1)U(\mathbf{r}_2)\rangle$$
$$= U_1^*(\mathbf{r}_1)U_1(\mathbf{r}_2) + U_2^*(\mathbf{r}_1)U_2(\mathbf{r}_2) + \cdots + U_p^*(\mathbf{r}_1)U_p(\mathbf{r}_2)$$
$$= \sum_n\sum_m \alpha_{1n}^*\alpha_{1m}\phi_n'^*(\boldsymbol{\rho}_1)\phi_m'(\boldsymbol{\rho}_2) + \sum_n\sum_m \alpha_{2n}^*\alpha_{2m}\phi_n'^*(\boldsymbol{\rho}_1)\phi_m'(\boldsymbol{\rho}_2) + \cdots$$
$$+\sum_n\sum_m \alpha_{pn}^*\alpha_{pm}\phi_n'^*(\boldsymbol{\rho}_1)\phi_m'(\boldsymbol{\rho}_2)$$
$$= \sum_n\sum_m\langle\alpha_n^*\alpha_m\rangle\phi_n^*(\mathbf{r}_1)\phi_m(\mathbf{r}_2)$$
$$= \sum_n \lambda_n\phi_n^*(\mathbf{r}_1)\phi_n(\mathbf{r}_2). \quad \text{(S14)}$$

Here p is the total number of modes U, $\lambda_n = \langle\alpha_n^*\alpha_n\rangle$, and $\langle\ \rangle$ means ensemble average. When the light source propagates through a unitary optical system, each mode evolves into

$$|U_i'\rangle = T|U_i\rangle = \sum_n \alpha_{in}T|\phi_n\rangle = \sum_n \alpha_{in}|\phi_n'\rangle. \quad \text{(S15)}$$

Similarly,

$$W_T(\boldsymbol{\rho}_1, \boldsymbol{\rho}_2) = \langle U'^*(\boldsymbol{\rho}_1) U'(\boldsymbol{\rho}_2) \rangle = \sum_n \lambda_n \phi_n'^*(\boldsymbol{\rho}_1) \phi_m'(\boldsymbol{\rho}_2). \quad \text{(S16)}$$

The mode-weights $\{\lambda_n\}$ are constant under the premise that matrix T does not change the orthogonal nature of the basis. Similarly, as discussed in Fig. 2 and Table 1, a wrong basis may affect the coherence entropy defined according to the mode-weights basis.

Example 1: Fraunhofer diffraction of a GSM.

The Fraunhofer diffraction and Fortier transform are typical unitary transformations. Considering the 1D Fraunhofer diffraction of Gaussian Shell modal (GSM) beam as an example, whose cross-spectral density is written as

$$W_0(x_1, x_2) = \exp\left(-\frac{x_1^2 + x_2^2}{4\sigma_0^2}\right) \exp\left[-\frac{(x_1 - x_2)^2}{2\delta_0^2}\right] = \sum_{n=0}^{\infty} \lambda_n \phi_n^*(x_1)\, \phi_n(x_2), \quad \text{(S17)}$$

where,

$$\phi_n(x) = \left(\frac{2c}{\pi}\right)^{1/4} \frac{1}{\sqrt{2^n n!}} H_n\left(\sqrt{2c}x\right) \exp(-cx^2),$$

$$\lambda_n = \left(\frac{\pi}{a+b+c}\right)^{1/2} \left(\frac{b}{a+b+c}\right)^n,$$

$$a = \frac{1}{4\sigma_0^2},\ b = \frac{1}{2\delta_0^2},\ \text{and}\ c = \sqrt{a^2 + 2ab}. \quad \text{(S18)}$$

On the far field plane:

$$W_T(\rho_1, \rho_2) = -\frac{\exp(i2kz)}{\lambda^2 z^2} \exp\left[\frac{ik}{2z}(\rho_1^2 + \rho_2^2)\right]$$

$$\times \int_{-\infty}^{\infty} \int_{-\infty}^{\infty} \mathrm{W}(x_1, x_2) exp\left[\frac{ik}{z}(x_1\rho_1 - x_2\rho_2)\right] dx_1 dx_2. \quad \text{(S19)}$$

After simple derivations and using the equation $\sum_{n=0}^{\infty} \frac{H_n(x)H_n(y)}{n!} t^n = (1 - 4t^2)^{-1/2} exp\left[y^2 - \frac{(y-2xt)^2}{1-4t^2}\right]$, $\mathrm{W}(\rho_1, \rho_2)$ can be simplified as

$$W(\rho_1, \rho_2) = -\frac{\pi}{c} \frac{\exp(i2kz)}{\lambda^2 z^2} \exp\left[\frac{ik}{2z}(\rho_1^2 + \rho_2^2)\right] \exp\left[-\frac{\rho_1^2 + \rho_2^2}{4\sigma_w{}^2}\right] \exp\left(-\frac{(\rho_1 - \rho_2)^2}{2\delta_w}\right), \quad \text{(S20)}$$

where $\sigma_w = \gamma\sigma_0$, $\delta_w = \gamma\delta_0$ and $\gamma = \frac{2cz}{k}$. Eq. (S20) can also be incoherently decomposed as $\mathrm{W}(\rho_1, \rho_2) = \sum_{n=0}^{\infty} \lambda_n \phi_n'^*(\rho_1)\, \phi_n'(\rho_2)$, where ϕ_n' has similar expressions as Eq. (S18):

$$\phi_n'(\rho_1) = \left(\frac{2c}{\pi}\right)^{1/4} \frac{1}{\sqrt{2^n n!}} \times H_n\left[-\sqrt{2c}\left(\frac{\rho_1}{\gamma}\right)\right] \exp\left[-c\left(\frac{\rho_2}{\gamma}\right)^2\right],$$

$$\lambda_n = \left(\frac{\pi}{a+b+c}\right)^{1/2} \left(\frac{b}{a+b+c}\right)^n,$$

$$a = \frac{1}{4\sigma_0^2},\ b = \frac{1}{2\delta_0^2},\ \text{and}\ c = \sqrt{a^2 + 2ab}. \quad \text{(S21)}$$

A comparison of Eq. (S18) and Eq. (S21) indicates that because of the unitary nature of the Fraunhofer transmission matrix T, ϕ_n' is simply scaled based on ϕ_n, and the mode-weight

λ_n is unchanged. The Fourier transform through a spherical lens exhibits a similar form as the Fraunhofer diffraction, and thus, the conclusion is similar. Note that this convenient calculation benefits from the clear mathematical model of the GSM beam. For partially coherent beams with more complex cross-spectral density, the theoretical solution cannot be easily derived. Thus, we propose the modal decomposition method and verify the accuracy with a simple GSM beam.

Example 2: cylindrical lens.

We consider the cylindrical lens as an example to show the flexibility of measurement. Owing to the transmission matrix T, each mode on the source plane $|U_i\rangle$ transforms to $|U_i^{SL}\rangle = T_{SL}|U_i\rangle$ for a spherical lens or $|U_i^{CL}\rangle = T_{CL}|U_i\rangle$ for a cylindrical lens system. In a two-dimensional case and spherical lens system, the modal decomposition on the source and focal plane for each mode can be written as

$$U_i(\mathbf{r}) = \sum_{n=1}^{N} \alpha_{ni}\phi_n(\mathbf{r}),$$
$$U_i^{SL}(\boldsymbol{\rho}) = \sum_{n=1}^{N_{sl}} \alpha_{ni}^{SL}\phi_n^{SL}(\boldsymbol{\rho}), \tag{S22}$$

where $N_{sl} = N$ is the total mode number, $\{\phi_n^{SL}\}$ is the basis fitted on the spherical lens focal plane, and $\alpha_{ni}^{SL} = \alpha_{ni}$ in spherical lens focusing. However, in a cylindrical lens system, both the simulation and experimental results, indicate that the intensities tilt into an elongated spot (see Fig. 2 in the main manuscript). If the differences between cylindrical lenses and spherical lenses, in addition to the tilt transformation of the light spot, are ignored and the basis is fitted using the beam waist and coherence along certain direction, the modal decomposition becomes

$$U_i^{CL}(\boldsymbol{\rho}) = \sum_{n=1}^{N_{cl}} \alpha_{ni}^{CL}\phi_n^{SL}(\boldsymbol{\rho}), \tag{S23}$$

where the basis $\{\phi_n^{SL}\}$ is consistent with Eq. (S22), while the mode number N_{cl} and the mode-weights α_{ni}^{CL} are changed, which may also result in a change in entropy. Although the basis can be chosen flexibly, there may be a distortion in mode-weights when choosing an inappropriate basis. Therefore, we apply transmission matrix T onto the source basis as $|\phi_n^{CL}\rangle = T_{CL}|\phi_n\rangle$ and the modal decomposition becomes

$$U_i^{CL}(\boldsymbol{\rho}) = \sum_{n=1}^{N'_{cl}} \alpha_{ni}'^{CL}\phi_n^{CL}(\boldsymbol{\rho}). \tag{S24}$$

Based on the aforementioned analysis, $\alpha_{ni}'^{CL} = \alpha_{ni}^{SL} = \alpha_{ni}$ and $N'_{cl} = N$ (no energy loss). Then, the final mode-weights are consistent with the source plane. The unitary nature of the channel ensures the orthogonality of the new basis after applying transmission matrix T on the original basis. More importantly, on the detection plane, we do not fix any aberrations in the light field but adjust the basis in modal decomposition calculation.

3. Modal decomposition in experiment.

When measuring a GSM, using the incoherent modal decomposition experimental method, a series of $\{U_i'(\boldsymbol{\rho})\}$ can be measured and further used in the calculation of $W_T(\boldsymbol{\rho}_1, \boldsymbol{\rho}_2)$. For a unitary optical system, such as Fraunhofer diffraction and Fourier transform, $|\phi_n'\rangle$ can be evaluated by applying the transmission matrix onto the original orthogonal basis. For a simple

case with theoretical solutions, the new basis on the output plane may be chosen by fitting $W_T(\boldsymbol{\rho}_1, \boldsymbol{\rho}_0)$ to obtain the beam and coherence widths. Then, the mode-weights can be measured by decomposing each sub-mode $U_i'(\boldsymbol{\rho})$ into a fitted basis $\phi_n'(\boldsymbol{\rho})$, written as

$$U_i'(\boldsymbol{\rho}) = \sum_{n=1}^{N} \alpha_{ni} \phi_n'(\boldsymbol{\rho}) \tag{S25}$$

where $\alpha_{ni} = \int_{-\infty}^{\infty} U_i'(\boldsymbol{\rho}) \phi_n'(\boldsymbol{\rho}) d\boldsymbol{\rho}$. In practical applications, it has finite integral boundary. Then, the cross-spectral density can be reorganized as

$$W_T(\boldsymbol{\rho}_1, \boldsymbol{\rho}_2) = \sum_{n=1}^{N} [\sum_{i=1}^{M} (\alpha_{ni})^2] \phi_n'^*(\boldsymbol{\rho}_1) \phi_n'(\boldsymbol{\rho}_2). \tag{S26}$$

Therefore, compared with Eq. (S6), the mode-weights λ_n can be calculated using

$$\lambda_n = \sum_{i=1}^{M} (\alpha_{ni})^2. \tag{S27}$$

The measurement with mode filters can easily show the spectrum of spatial modes and vector nature of the coherent beam but cannot efficiently reconstruct the entire BCP matrix (discussed in Section II) and perform inverse operation.

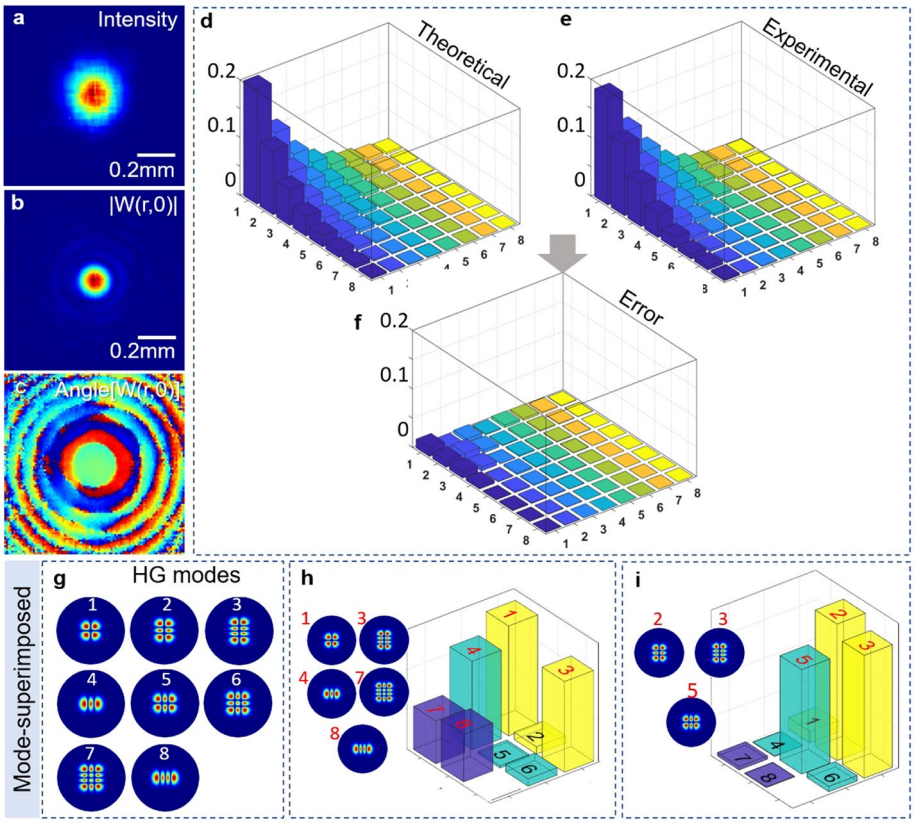

Fig. S1. Intensity, cross spectral density (CSD) and mode-weight calculated from measured mixed modes. (a-c) Intensity, amplitude and phase of cross-spectral density of a GSM beam focused by a spherical lens; GSM mode-weights calculated with (d) Eq. (S21) (theoretical mode-weights) and (e) Eq. (5) (experimentally decomposed mode-weights); (f) mode-weights measurement error. The source coherence width and beam waist are set as $\delta_0 = 0.58 w_0$ and $w_0 = 1$ mm, respectively. (g) HG eigen modes used for superposing a random beam. (h, i) Two examples of modal superposition. (left) Modes used and (right) corresponding experimentally measured mode-weights.

We consider the spherical lens system as an example. The focused cross-spectral density (measurement target) of a GSM is calculated with $W_f(\boldsymbol{\rho}_1, \boldsymbol{\rho}_2) = \sum_{t=1}^{M} P_t^*(\boldsymbol{\rho}_1) P_t(\boldsymbol{\rho}_2)$, where $\boldsymbol{\rho}$ denotes the coordinate on the focal plane and $\{P_t(\boldsymbol{\rho})\}$ are the measured modes in the focal plane. Fig. S1a-c show the intensity and cross-spectral density results of the focused GSM. As shown in Fig. S1d, the theoretical mode-weights can then be calculated by fitting the focal coherence width and beam waist. The experimentally decomposed mode-weights are shown in Fig. S1e. As shown in Fig. S1f, the difference between these two mode-weights results is considerably smaller than the mode-weights. This means that the theoretically fitted and experimentally decomposed mode-weights results are nearly equivalent. However, compared with theoretical mode-weights calculation, the experimentally decomposed mode-weights are model independent. This feature is shown in Fig. S1g-i, which demonstrates the mode-weights measurement results of two randomly superposed beams. The Gaussian amplitude filter in Fig. 1 is replaced with a spatial light modulator, which is used to load HG modes modulation masks (eight modes in total), shown in Fig. S1g. Two examples are given in Fig. S1h,i. The mode-weights (shown in bars) calculated using the mixed modes agree with that actually used for superposition.

II. Vector partially coherent beam

For a vector partially coherent beam, the properties can be analyzed using the BCP matrix, written as

$$\mathbf{W}(\mathbf{r}_1, \mathbf{r}_2) = \begin{bmatrix} W_{uu}(\mathbf{r}_1, \mathbf{r}_2) & W_{uv}(\mathbf{r}_1, \mathbf{r}_2) \\ W_{vu}(\mathbf{r}_1, \mathbf{r}_2) & W_{vv}(\mathbf{r}_1, \mathbf{r}_2) \end{bmatrix}, \tag{S28}$$

where u and v are the generic orthogonal polarization states and simplified in the following analysis as polarizations along x and y directions, that is horizontal and vertical polarization states:

$$\mathbf{W}(\mathbf{r}_1, \mathbf{r}_2) = \begin{bmatrix} W_{xx}(\mathbf{r}_1, \mathbf{r}_2) & W_{xy}(\mathbf{r}_1, \mathbf{r}_2) \\ W_{yx}(\mathbf{r}_1, \mathbf{r}_2) & W_{yy}(\mathbf{r}_1, \mathbf{r}_2) \end{bmatrix} = \begin{bmatrix} \langle E_x^*(\boldsymbol{r}_1) E_x(\boldsymbol{r}_2) \rangle & \langle E_x^*(\boldsymbol{r}_1) E_y(\boldsymbol{r}_2) \rangle \\ \langle E_y^*(\boldsymbol{r}_1) E_x(\boldsymbol{r}_2) \rangle & \langle E_y^*(\boldsymbol{r}_1) E_y(\boldsymbol{r}_2) \rangle \end{bmatrix}. \tag{S29}$$

In general, the modal decomposition of a partially polarized and partially coherent beam can be expressed as[32,33]:

$$\boldsymbol{W}(\mathbf{r}_1, \mathbf{r}_2) = \sum_n \Lambda_n \boldsymbol{\Phi}_n^{\dagger}(\mathbf{r}_1) \boldsymbol{\Phi}_n(\mathbf{r}_1), \tag{S30}$$

where the eigenmodes have the vector form $\boldsymbol{\Phi}_n(\mathbf{r}) = \begin{pmatrix} \Phi_{n;u}(\mathbf{r}) \\ \Phi_{n;v}(\mathbf{r}) \end{pmatrix}$, Λ_n denotes eigenvalues, and the dagger "†" represents the Hermitian conjugate. Gori[2] theoretically showed that the modal decomposition of a partially polarized and partially coherent light source could be achieved by solving a pair of coupled integral equations:

$$\sum_{\xi} \int \boldsymbol{W}_{\eta,\xi}(\mathbf{r}_1, \mathbf{r}_2) \Phi_{n;\xi}(\mathbf{r}_1) \mathrm{d}^2\mathbf{r}_1 = \Lambda_n \Phi_{n;\eta}(\mathbf{r}_2), (\eta; \xi = u, v). \tag{S31}$$

In general, solving Eq. (S31) may be nontrivial. Thus, we suppose that the modes in two polarization components construct a complete set of orthogonal spatial basis. Furthermore, we only consider a vector partially coherent beam with diagonal BCP matrix, whose modal

decomposition can be simplified as that of a scalar cross-spectral density defined with $W_{eq} = W_{xx} + W_{yy}$[33]. Thus, the conclusion about coherence entropy will be consistent with that of scalar beam.

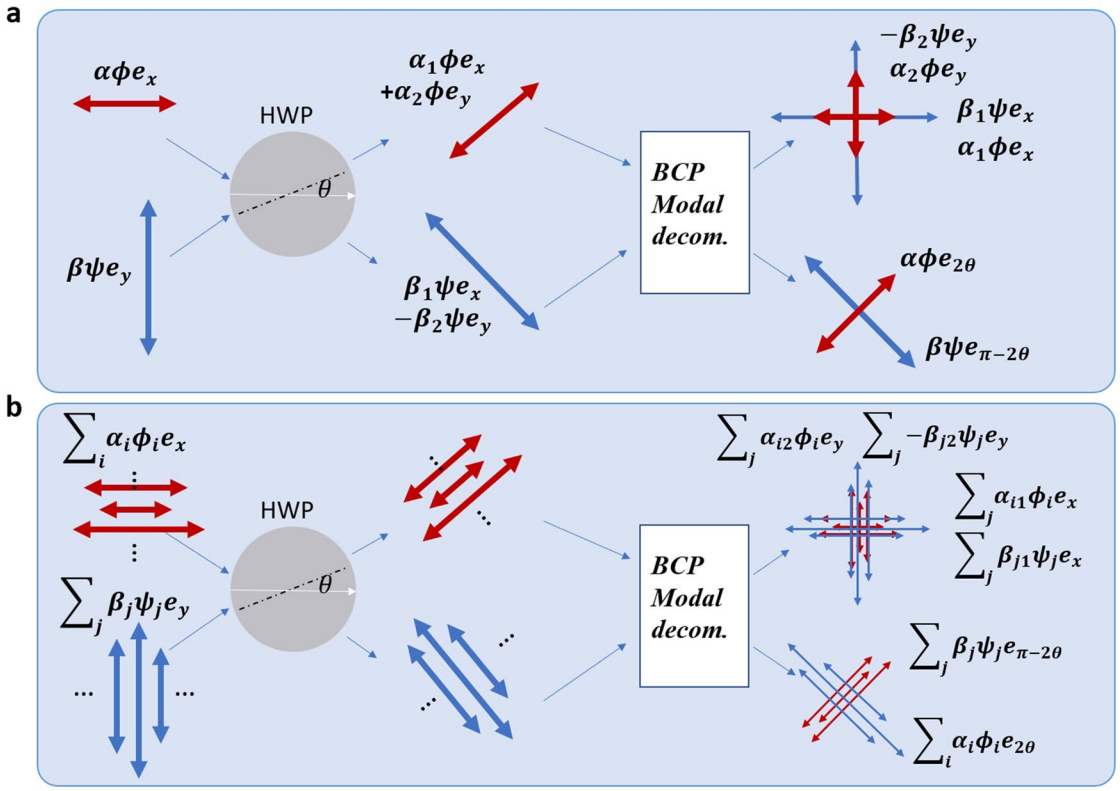

Fig. S2. Modal decomposition of a (a) vector beam and (b) partially coherent vector beam after passing through a half-wave-plate (HWP).

Considering a vector light source composed of two single-mode polarization components (see Fig. S2a), the BCP matrix on the source plane can be written as

$$\boldsymbol{W_0}(\mathbf{r}_1, \mathbf{r}_2) = \begin{bmatrix} W_{xx}(\mathbf{r}_1, \mathbf{r}_2) & W_{xy}(\mathbf{r}_1, \mathbf{r}_2) \\ W_{yx}(\mathbf{r}_1, \mathbf{r}_2) & W_{yy}(\mathbf{r}_1, \mathbf{r}_2) \end{bmatrix}$$

$$= \begin{bmatrix} \langle \alpha^* \alpha \rangle \phi^*(\boldsymbol{r}_1)\phi(\boldsymbol{r}_2) & \langle \alpha^* \beta \rangle \phi(\boldsymbol{r}_1)\psi(\boldsymbol{r}_2) \\ \langle \beta^* \alpha \rangle \psi^*(\boldsymbol{r}_1)\phi(\boldsymbol{r}_2) & \langle \beta^* \beta \rangle \psi^*(\boldsymbol{r}_1)\psi(\boldsymbol{r}_2) \end{bmatrix}. \quad \text{(S32)}$$

Here, the coefficient is statistically independent, i.e., $\langle \alpha^* \beta \rangle = \langle \beta^* \alpha \rangle = 0$, and thus, the BCP matrix becomes diagonal, as shown below:

$$\boldsymbol{W_0}(\mathbf{r}_1, \mathbf{r}_2) = \begin{bmatrix} \lambda_{xx}\phi^*(\boldsymbol{r}_1)\phi(\boldsymbol{r}_2) & 0 \\ 0 & \lambda_{yy}\psi^*(\boldsymbol{r}_1)\psi(\boldsymbol{r}_2) \end{bmatrix}. \quad \text{(S33)}$$

For each polarization component, the light field is coherent and the mode-weight is single valued, that is $\lambda_{xx} = \langle \alpha^* \alpha \rangle$, $\lambda_{xy} = 0$, $\lambda_{yx} = 0$ and $\lambda_{yy} = \langle \beta^* \beta \rangle$. As shown in Fig. S2a, taking the half-wave-plate as an example, which is a typical unitary transform, the Jones matrix is written as

$$J_{HWP} = \begin{bmatrix} cos^2\theta - sin^2\theta & 2sin\theta cos\theta \\ 2sin\theta cos\theta & sin^2\theta - cos^2\theta \end{bmatrix} = \begin{bmatrix} cos2\theta & sin2\theta \\ sin2\theta & -cos2\theta \end{bmatrix}. \quad \text{(S34)}$$

The output BCP matrix can be calculated as

$$\boldsymbol{W}(\boldsymbol{\rho}_1, \boldsymbol{\rho}_2) = \begin{bmatrix} W_{xx}(\boldsymbol{\rho}_1, \boldsymbol{\rho}_2) & W_{xy}(\boldsymbol{\rho}_1, \boldsymbol{\rho}_2) \\ W_{yx}(\boldsymbol{\rho}_1, \boldsymbol{\rho}_2) & W_{yy}(\boldsymbol{\rho}_1, \boldsymbol{\rho}_2) \end{bmatrix} =$$

$$\begin{bmatrix} \langle \alpha_1^* \alpha_1 \rangle \phi^*(\boldsymbol{\rho}_1)\phi(\boldsymbol{\rho}_2) + \langle \beta_1^* \beta_1 \rangle \psi^*(\boldsymbol{\rho}_1)\psi(\boldsymbol{\rho}_2) & \langle \alpha_1^* \alpha_2 \rangle \phi^*(\boldsymbol{\rho}_1)\phi(\boldsymbol{\rho}_2) - \langle \beta_1^* \beta_2 \rangle \psi^*(\boldsymbol{\rho}_1)\psi(\boldsymbol{\rho}_2) \\ \langle \alpha_2^* \alpha_1 \rangle \phi^*(\boldsymbol{\rho}_1)\phi(\boldsymbol{\rho}_2) - \langle \beta_2^* \beta_1 \rangle \psi^*(\boldsymbol{\rho}_1)\psi(\boldsymbol{\rho}_2) & \langle \alpha_2^* \alpha_2 \rangle \phi^*(\boldsymbol{\rho}_1)\phi(\boldsymbol{\rho}_2) + \langle \beta_2^* \beta_2 \rangle \psi^*(\boldsymbol{\rho}_1)\psi(\boldsymbol{\rho}_2) \end{bmatrix}. \quad \text{(S35)}$$

The mode-weights of the four components in BCP matrix are $\lambda_{xx} = \{\langle \alpha_1^* \alpha_1 \rangle, \langle \beta_1^* \beta_1 \rangle\}$, $\lambda_{yy} = \{\langle \alpha_2^* \alpha_2 \rangle, \langle \beta_2^* \beta_2 \rangle\}$, $\lambda_{xy} = \{\langle \alpha_1^* \alpha_2 \rangle, -\langle \beta_1^* \beta_2 \rangle\}$, and $\lambda_{xy} = \{\langle \alpha_2^* \alpha_1 \rangle, -\langle \beta_2^* \beta_1 \rangle\}$, where $\alpha_1^2 + \alpha_2^2 = \alpha^2$ and $\beta_1^2 + \beta_2^2 = \beta^2$. Other cross terms were omitted owing to uncorrelated coefficients. Compared with the source plane, the mode-weights for each component change. However, the mode-weights for each component will be consistent if the decomposition vector basis is adjusted. As shown in Fig. S2a, the BCP matrix on the output plane can be written as

$$\begin{aligned} \boldsymbol{W}(\boldsymbol{\rho}_1, \boldsymbol{\rho}_2) &= \begin{bmatrix} W_{2\theta,2\theta}(\boldsymbol{\rho}_1, \boldsymbol{\rho}_2) & W_{2\theta,\pi-2\theta}(\boldsymbol{\rho}_1, \boldsymbol{\rho}_2) \\ W_{\pi-2\theta,2\theta}(\boldsymbol{\rho}_1, \boldsymbol{\rho}_2) & W_{\pi-2\theta,\pi-2\theta}(\boldsymbol{\rho}_1, \boldsymbol{\rho}_2) \end{bmatrix} \\ &= \begin{bmatrix} \langle \alpha^* \alpha \rangle \phi^*(\boldsymbol{\rho}_1)\phi(\boldsymbol{\rho}_2) & 0 \\ 0 & \langle \beta^* \beta \rangle \psi^*(\boldsymbol{\rho}_1)\psi(\boldsymbol{\rho}_2) \end{bmatrix}. \end{aligned} \quad \text{(S36)}$$

More specific examples have been clearly discussed previously[32], wherein the authors state that the BCP matrix can be transformed into diagonal version by choosing a new reference frame. Similarly, for a vector partially coherent beam with more spatial modes for each polarization component,

$$\boldsymbol{W_0}(\mathbf{r}_1, \mathbf{r}_2) = \begin{bmatrix} \sum_i \lambda_i \phi_i^*(\mathbf{r}_1)\phi_i(\mathbf{r}_2) & 0 \\ 0 & \sum_j \mu_j \psi_j^*(\mathbf{r}_1)\psi_j(\mathbf{r}_2) \end{bmatrix}. \quad \text{(S37)}$$

On the output plane, by adjusting the basis ($[\phi_i, e_x; \psi_j, e_y]$ into $[\phi_i', e_u; \psi_j', e_v]$) (see Fig. S2b for an example), the BCP matrix becomes

$$\begin{aligned} \boldsymbol{W}(\boldsymbol{\rho}_1, \boldsymbol{\rho}_2) &= \begin{bmatrix} W_{uu}(\boldsymbol{\rho}_1, \boldsymbol{\rho}_2) & W_{uv}(\boldsymbol{\rho}_1, \boldsymbol{\rho}_2) \\ W_{vu}(\boldsymbol{\rho}_1, \boldsymbol{\rho}_2) & W_{vv}(\boldsymbol{\rho}_1, \boldsymbol{\rho}_2) \end{bmatrix} \\ &= \begin{bmatrix} \sum_i \lambda_i \phi_i'^*(\boldsymbol{\rho}_1)\phi_i'(\boldsymbol{\rho}_2) & 0 \\ 0 & \sum_i \mu_j \psi_j'^*(\boldsymbol{\rho}_1)\psi_j'(\boldsymbol{\rho}_2) \end{bmatrix}. \end{aligned} \quad \text{(S38)}$$

Therefore, if the optical system is unitary and the BCP matrix is initially diagonal, the overall mode-weight $\lambda = \lambda_{xx} + \lambda_{yy} + \lambda_{xy} + \lambda_{yx}$ of a vector partially coherent beam will be constant when an appropriate basis (i.e., including spatial basis and vector basis) is chosen. The experimental decomposition may be achieved with the modal decomposition method proposed in this study.

Experimental BCP modal decomposition. Considering Fig. S2a as an example, if the modal decomposition is performed by choosing *x* and *y* polarization basis, the modal decomposition

will be complicated owing to the coupling of two polarization components. By choosing a new set of vector basis, the problem reduces to two scalar modal decomposition problems. Note that, the modal decomposition proposed in this study is not sensitive to the polarization. In the other words, for an initially diagonal case, two components of the BCP matrix, that is the equivalent scalar cross-spectral density W_{eq}, can be decomposed together. If required, the modal decomposition for each component may be achieved using a linear polarizer. Then, the modal decomposition can be applied to demonstrate more complex entropy conversion cases discussed previously[28-30].

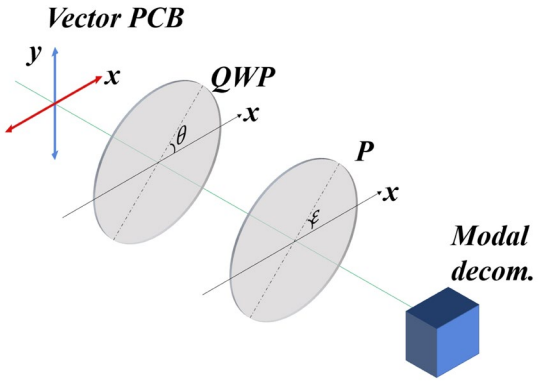

Fig. S3. BCP modal decomposition. Schematic of BCP measurement for the input vector partially coherent beam. PCB, partially coherent beam; QWP, quarter-wave plate; P, polarizer.

For non-diagonal case, overall modal decomposition may be achieved when two polarization components share the same set of orthogonal spatial basis. As shown in Fig. S3, corresponding $W_{\theta,\varepsilon}$ can be measured by rotating the quarter-wave plate and the linear polarizer as

$$W_{\theta,\varepsilon} = W_{xx}\cos^2\theta + W_{xy}\exp(-i\varepsilon)\cos\theta\sin\theta + W_{yx}\exp(i\varepsilon)\cos\theta\sin\theta + W_{yy}\sin^2\theta. \quad \text{(S39)}$$

Here, θ represents the angle between the x-axis and the quarter-wave plate's fast axis, which induces a phase delay between the x and y components of the incident stochastic electromagnetic beam. Here, ε denotes the angle between the linear polarizer and x-axis. For example, $W_{xx}(\mathbf{r}_1,\mathbf{r}_2)$ and $W_{yy}(\mathbf{r}_1,\mathbf{r}_2)$ can be measured by performing modal decomposition after a quarter-wave plate and linear polarizer, where the linear polarizer angle and quarter-wave plate fast axis are both parallel to x ($\theta = 0$ and $\varepsilon = 0$) for $W_{xx}(\mathbf{r}_1,\mathbf{r}_2)$ and y ($\theta = \pi/2$ and $\varepsilon = \pi/2$) for $W_{yy}(\mathbf{r}_1,\mathbf{r}_2)$. For other components, four measurement iterations (modal decomposition) are required:

$$W_{xy}(\mathbf{r}_1,\mathbf{r}_2) = \frac{1}{2}\left\{\left[W_{\frac{\pi}{4},0}(\mathbf{r}_1,\mathbf{r}_2) - W_{\frac{3\pi}{4},0}(\mathbf{r}_1,\mathbf{r}_2)\right] + i\left[W_{\frac{\pi}{4},\frac{\pi}{2}}(\mathbf{r}_1,\mathbf{r}_2) - W_{\frac{3\pi}{4},\frac{\pi}{2}}(\mathbf{r}_1,\mathbf{r}_2)\right]\right\},$$

$$W_{yx}(\mathbf{r}_1,\mathbf{r}_2) = \frac{1}{2}\left\{\left[W_{\frac{\pi}{4},0}(\mathbf{r}_1,\mathbf{r}_2) - W_{\frac{3\pi}{4},0}(\mathbf{r}_1,\mathbf{r}_2)\right] - i\left[W_{\frac{\pi}{4},\frac{\pi}{2}}(\mathbf{r}_1,\mathbf{r}_2) - W_{\frac{3\pi}{4},\frac{\pi}{2}}(\mathbf{r}_1,\mathbf{r}_2)\right]\right\}. \quad \text{(S40)}$$

By substituting Eq. (S39) into Eq. (S40), the mode-weights of four components in the BCP matrix can be calculated.

Supplemental figures

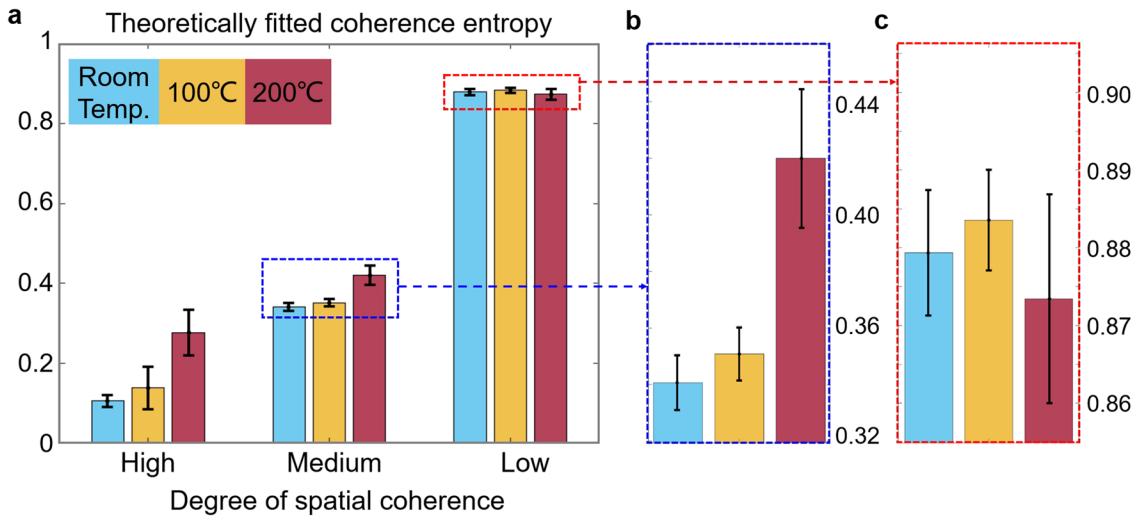

Fig. S4. Theoretically fitted coherence entropy of a GSM beam passing through the turbulent atmosphere system. (b, c) show the enlarged field of view of medium-coherence and low-coherence cases in (a).

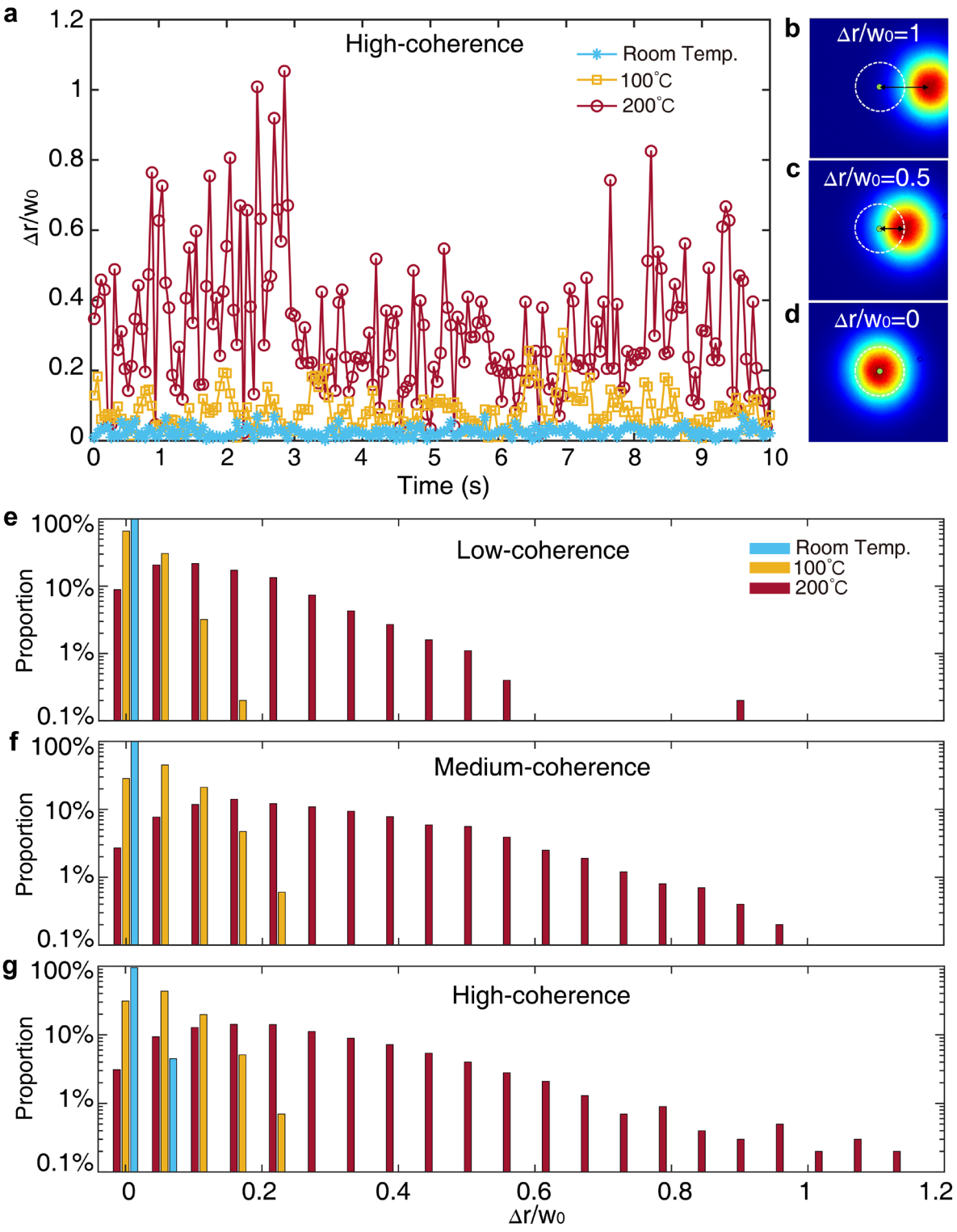

311

312 **Fig. S5.** Beam wander of three kinds of turbulence for various degrees of coherence. (a) Each
313 frame has an exposure time of 3 ms, and 200 images are recorded within 10 s. The beam wander
314 is defined according to the ratio of beam drift Δr relative to beam width w_0 and (b-d) show the
315 diagrams of $\Delta r/w_0$ =0, 0.5, and 1. Green dot marks the coordinate center. Y-scale for (e-g) is
316 log scale. The range of schematic diagrams (d-f) is not the real size of measurement range in
317 modal decomposition.
318

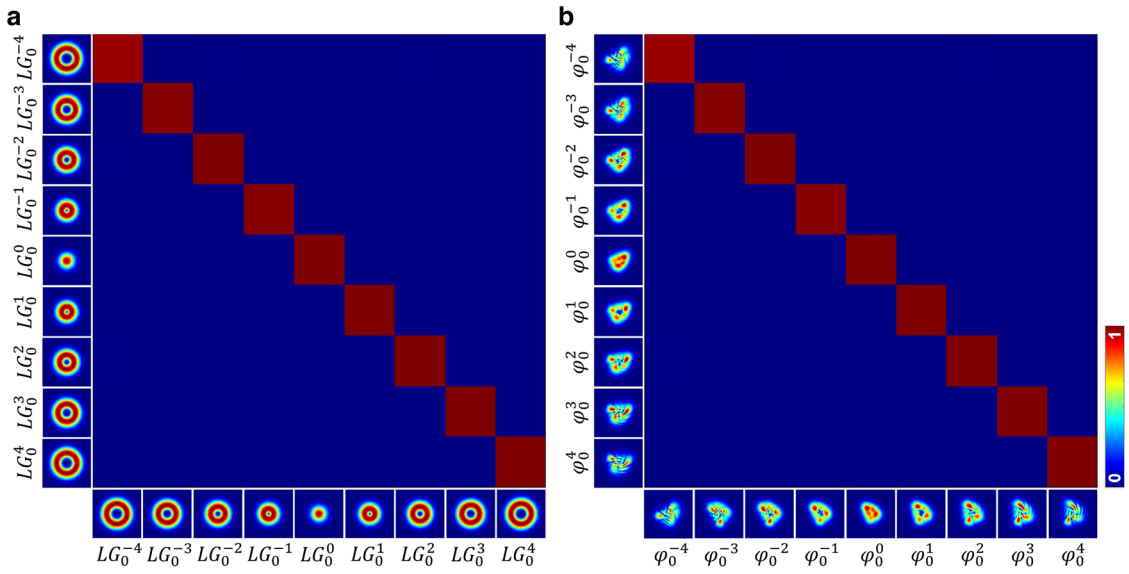

319

320 **Fig. S6.** Simulated cross-talk matrices of Laguerre Gaussian modes on the (a) source plane
321 and (b) after turbulent media.

322

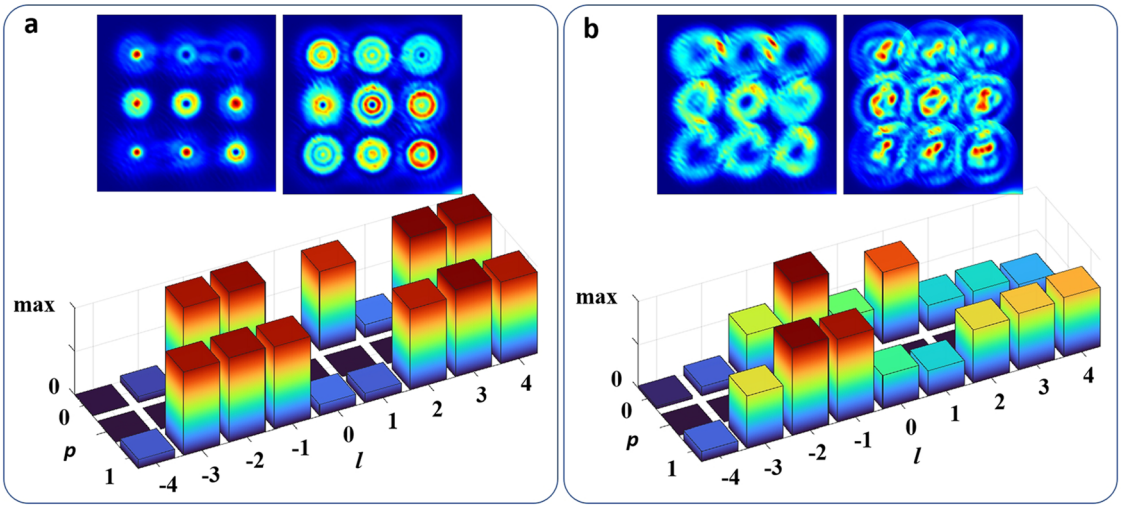

323

324 **Fig. S7.** Simulation results of demultiplexing using multifocal array. Intensity patterns and
325 corresponding reconstructed mode-weights (a) in free space and (b) through turbulent media.

326

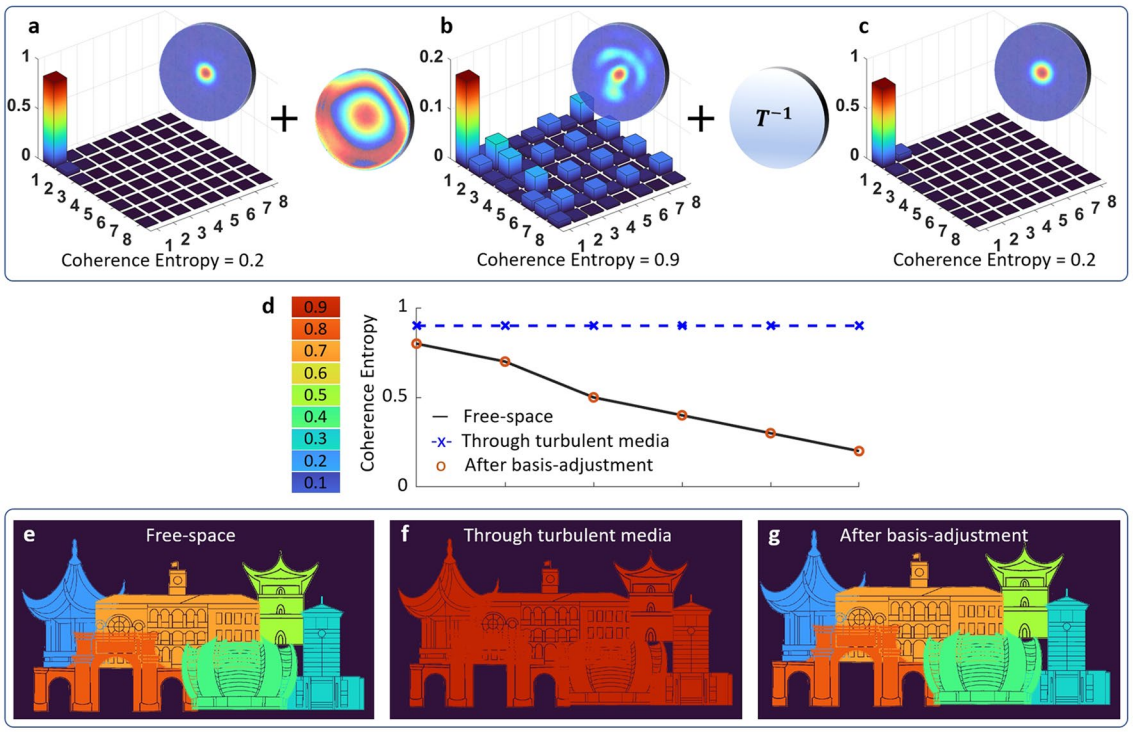

Fig. S8. Channel robustness using the conservation of coherence entropy. The incoherence decomposition basis is replaced with the HG modes and the other settings are the same as Fig. 5.